

Supplementary Material for

smiFISH and FISH-quant - a flexible single RNA detection approach with super-resolution capability

Nikolay Tsanov^{1,^}, Aubin Samacoits^{2,3,^}, Racha Chouaib^{1,4,^}, Abdel-Meneem Traboulsi¹, Thierry Gostan¹, Christian Weber^{2,3}, Christophe Zimmer^{2,3}, Kazem Zibara^{4,5}, Thomas Walter^{6,7,8}, Marion Peter^{1*}, Edouard Bertrand^{1*}, Florian Mueller^{2,3*}

¹ Institut de Génétique Moléculaire de Montpellier, UMR 5535 CNRS, 1919 route de Mende, 34293 Montpellier cedex 5, France; Université de Montpellier, 163 rue Auguste Broussonnet, 34090 Montpellier, France

² Unité Imagerie et Modélisation, Institut Pasteur and CNRS UMR 3691; 28, rue du Docteur Roux; 75015 Paris, France

³ C3BI, USR 3756 IP CNRS – Paris, France

⁴ ER045, Laboratory of Stem Cells, DSST, PRASE, Lebanese University, Beirut, Lebanon

⁵ Biology Department, Faculty of Sciences-I, Lebanese University, Beirut, Lebanon

⁶ MINES ParisTech, PSL-Research University, CBIO-Centre for Computational Biology, 77300 Fontainebleau, France

⁷ Institut Curie, 75248 Paris Cedex, France

⁸ INSERM, U900, 75248 Paris Cedex, France

[^] These authors contributed equally.

* Correspondence to: Marion Peter (marion.peter@igmm.cnrs.fr), Edouard Bertrand (edouard.bertrand@igmm.cnrs.fr), Florian Muller (fmuller@pasteur.fr)

1. Supplementary Figures and Table	2
Supplementary Figure S1	2
Supplementary Figure S2	4
Supplementary Figure S3	6
Supplementary Figure S4	7
Supplementary Figure S5	8
Supplementary Figure S6	9
Supplementary Table 1	11
2. Supplementary Protocol: mRNA detection with smiFISH	12
3. Note 1: sequences of FLAP probes	15
4. Note 2: Oligostan – R script for probe design	16
5. Note 3: fully automated analysis workflow for smFISH images in	17
Overview	17
Improved cell segmentation by focus based projection	17
Comparison of spot detection methods	24
Summary	28
6. References	29

1. Supplementary Figures and Table

Supplementary Figure S1

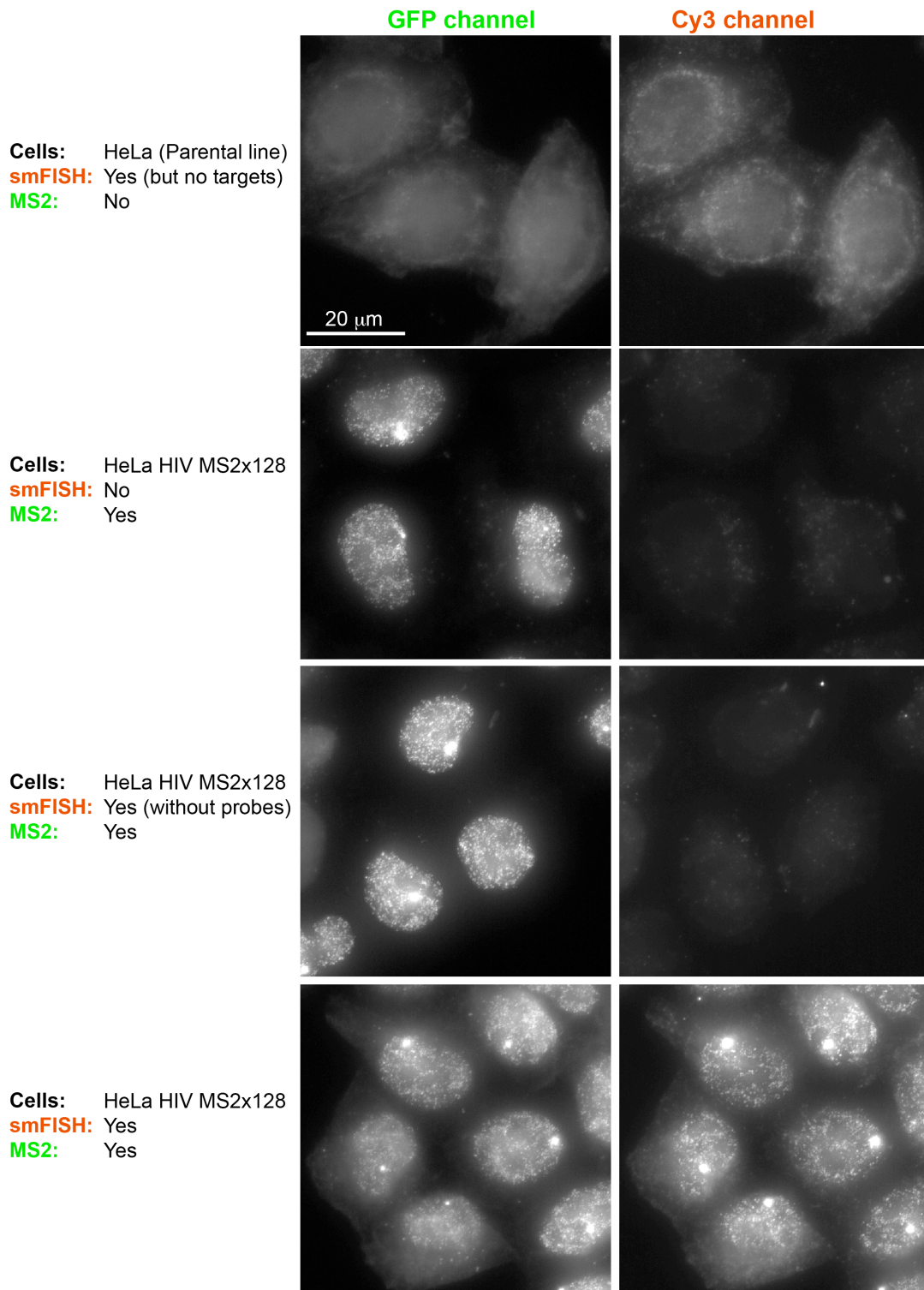


Figure S1: Control experiments for dual-colour experiments smiFISH-Cy3 and MS2-GFP targeting the same HIV reporter RNA. Each row corresponds to one dual-colour experiment. Row 1: no Cy3 and GFP signal detected in absence of reporter. Row 2 & 3: no bleed-through of GFP into Cy3 detected when either no smiFISH (row 2) or smiFISH without labelled probes (row 3) was performed. Row 4: GFP and Cy3 signal detected. All GFP images were acquired with identical acquisition

settings and are shown with same scaling, all Cy3 images were acquired with identical acquisition settings and are shown with same scaling. Same scale bar for all images.

Supplementary Figure S2

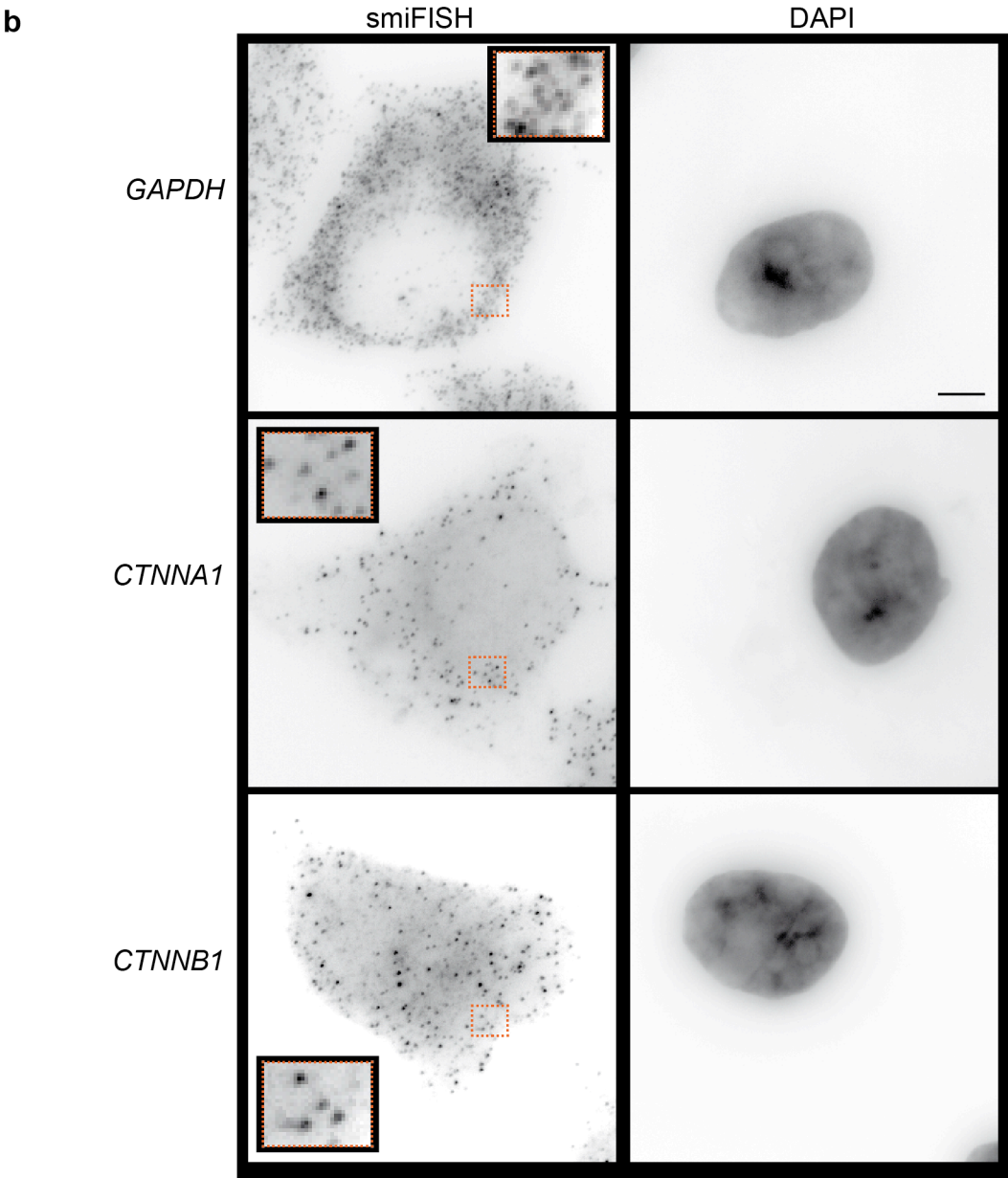
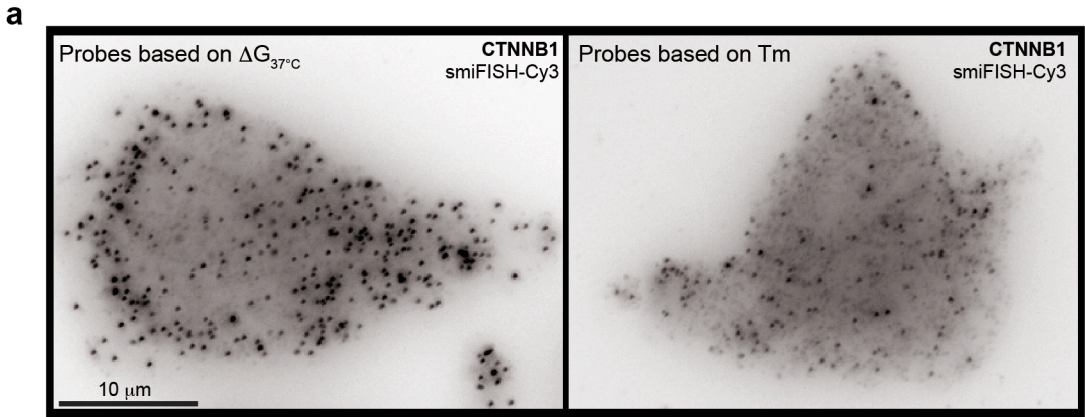


Figure S2: Detection of endogenous mRNA by smiFISH. **(a)** Comparison of smiFISH results obtained with probes whose design was based either on shared T_m or $\Delta G_{37^\circ C}$. smiFISH was performed against CTNNB1 in HeLa cells with sets of 24 primary probes hybridized with FLAP-Cy3 secondary probes. Images were acquired with identical acquisition settings. Images are maximum intensity projections and are shown with same scaling. Image on the left with probes designed with a shared $\Delta G_{37^\circ C}$, image on the right with shared T_m . Images have comparable background, but probes designed with shared $\Delta G_{37^\circ C}$ yield brighter spots corresponding to individual mRNA molecules, as also revealed by a higher Signal-To-Noise-Ratio (SNR; see Supplementary Table 1). **(b)** HeLa cells were hybridized with sets of 24 smiFISH probes whose design was based on shared $\Delta G_{37^\circ C}$, targeting genes with various expression levels: GAPDH (high), CTNNA1, CTNNB1 (intermediate). FLAP Y-Cy3 was used in all cases. Left: smiFISH images. Insets show zoom-in for dashed rectangles. Right: DAPI. Scale bar (same for all panels): 5 μm .

Supplementary Figure S3

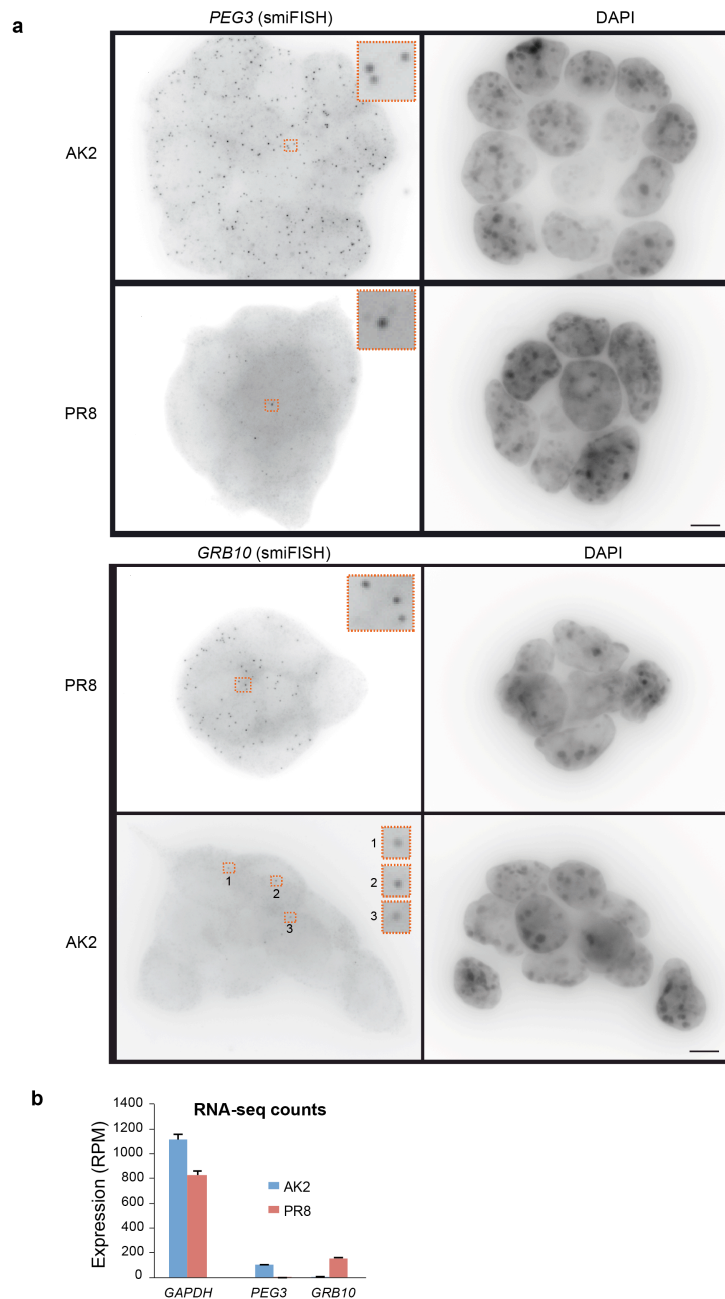


Figure S3: Detection of endogenous mRNAs with smiFISH. **(a)** The expression of *Peg3* and *Grb10*, two genes expressed in a parent-of-origin-specific manner, was analysed in monoparental androgenetic (AK2) and parthenogenetic (PR8) mES cells. Cells were hybridized with a set of 24 smiFISH probes targeting either *Peg3* or *Grb10*. FLAP X-Cy3 was used in both cases. Insets show a zoom-in for the regions indicated with the dashed rectangles. Scale bar: 5 μ m. **(b)** Expression of *Peg3*, *Grb10* and *GAPDH* in AK2 and PR8 cells characterized by RNA sequencing (RNA-seq). RNA-seq was performed in triplicates. 41 to 59 millions of reads per replicate were obtained in AK2 cells. 48 to 57 millions of reads per replicate were obtained in PR8 cells. RPM: reads per million. Data courtesy of Robert Feil laboratory (IGMM, Montpellier).

Supplementary Figure S4

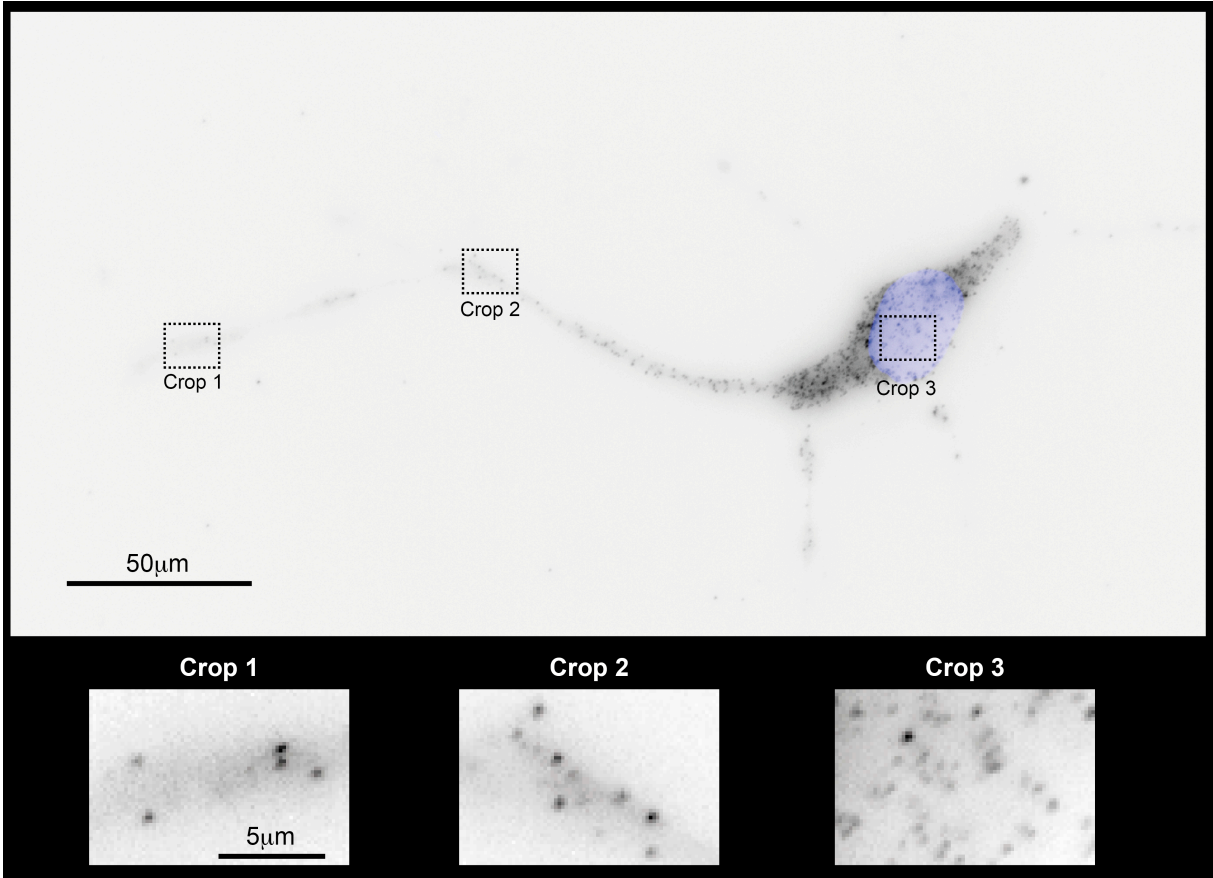


Figure S4: Detection of β -actin mRNA in neurons. (**Upper panel**) smiFISH is shown in black, and API as an overlay in blue. Contrast of smiFISH image is adjusted such that denser area in the cell body is not saturated. Scale bar as indicated. (**Lower panels**) show a zoom-in in the region indicated with dashed rectangles in the upper panel. Contrast of each image has been adjusted separately. Same scale bar for all three images.

Supplementary Figure S5

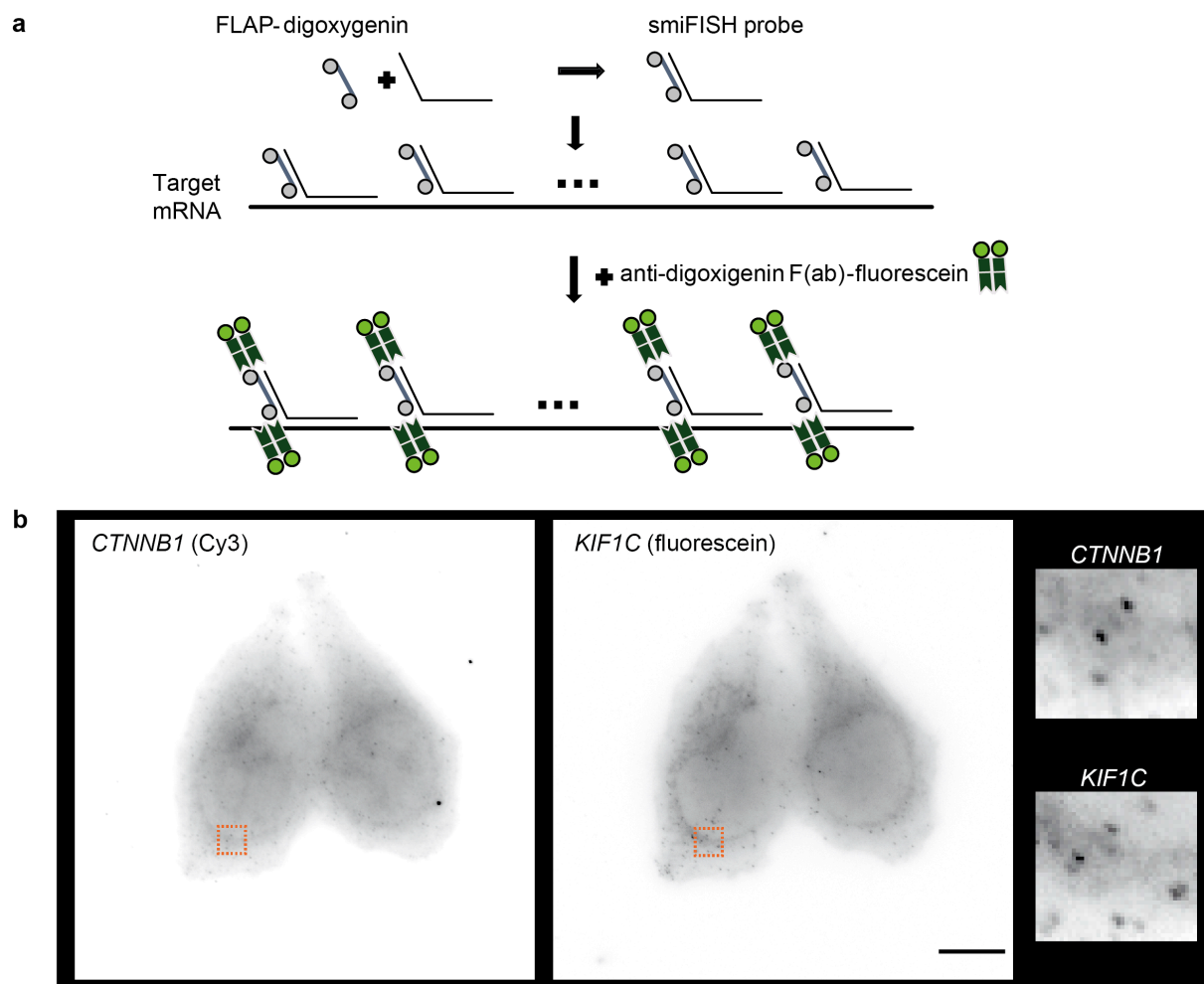


Figure S5: Detection of mRNA by two-colour smiFISH. **(a)** Principle of smiFISH combined with immunodetection. The FLAP conjugated to digoxigenin is first hybridized with 24 primary probes (FLAP hybridization step). The FLAP-structured duplexes (smiFISH probes) are subsequently hybridized to cells, before incubation with anti-digoxigenin Fab fragments labelled with fluorescein. Grey circles: digoxigenin moieties; green circles: fluorescein moieties. **(b)** Detection of CTNNB1 and KIF1C endogenous mRNA. HeLa cells were hybridized with sets of 24 smiFISH probes targeting CTNNB1 and KIF1C. Left column: mRNA detected with FLAP Y-Cy3 (as in Figure 1). Middle column: mRNA detected with FLAP Y-digoxigenin and anti-digoxigenin Fab-fluorescein (as presented in a). Scale bar: 5 μ m.

Supplementary Figure S6

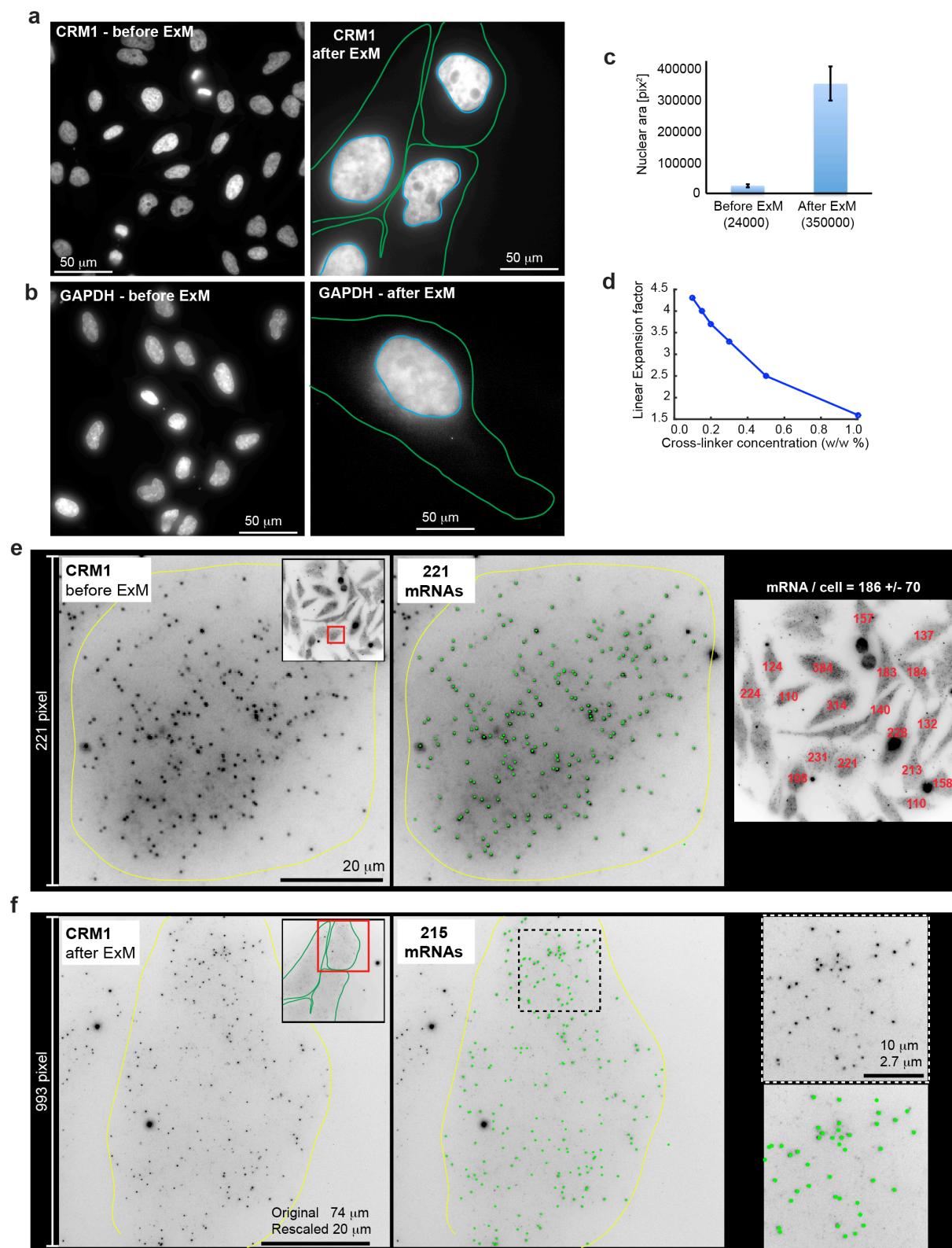


Figure S6: Expansion microscopy with smiFISH. (a,b) DAPI images for the smiFISH images in Fig. 4b. **e.** Note that images are scaled differently before and after expansion (images after expansion are substantially dimmer). **(c)** Mean and standard deviation of nuclear area in HeLa cells before ($N = 120$

cells) and after ($N=12$ cells) expansion. Mean area is 14 times larger after expansion, yielding a linear expansion factor of 3.7. Expansion was performed with a cross-linker concentration of 0.2%. **(d)** Linear expansion of specimen free gels with different cross-linker concentrations. **(e)** mRNA detection for CRM1 before ExM for cells shown in main Fig. 2b. Images are maximum intensity projections along Z (inset shows cropped cell). Green dots mark detected mRNAs. Plot on the right shows mRNA count for each cell in red, and average \pm standard count is reported. **(f)** mRNA detection for CRM1 after ExM for one cell shown in main Fig. 2b. Size of cropping region is matched to region used in (e) with consideration of the measured expansion factor. Size of cropping region is identical after considering the measured expansion factor from specimen-free gel for the ExM image and is therefore smaller for images before ExM. Please note that for the ExM images substantially more pixels are in the cropped region and the spots therefore appear smaller. Dashed rectangle indicates a region for which an inset is shown.

Supplementary Table 1

Gene name	Manual signal evaluation		Signal quantification [SNR]	
	Based on Tm	Based on $\Delta G_{37^\circ\text{C}}$	Based on Tm	Based on $\Delta G_{37^\circ\text{C}}$
CRM1	+	+	8.2	9.3
CTNNB1	+	++	7.9	13.5
DYNC1I2	no signal	+	-	-
DYNC1LI1	no signal	+	-	-
DYNC1LI2	+	++	6.1	6.9
DYNC2LI1	no signal	+	-	-
KIF1C	+	++	21.3	25

Supplementary Table 1: Comparison of smiFISH signals obtained with probes designed with either a shared Tm or $\Delta G_{37^\circ\text{C}}$. smFISH experiments were performed in HeLa cells with sets of 24 primary probes hybridized with FLAP-Cy3 secondary probe. **Manual signal evaluation:** samples were rated as follows. “no signal”: no mRNA spots visible. “+”: mRNA spots were visible. “++”: mRNA spots are easily visible. **Signal quantification:** Signal-to-noise ratio SNR was calculated as μ / σ , where μ is the mean of the FISH signal and σ is the standard deviation of the background. μ was obtained by averaging the estimated amplitude after fitting individual mRNA molecules with a Gaussian function with FISH-quant (1). σ was obtained by selecting parts of image with no RNA and only cellular background and calculating the standard deviation of the intensity. SNR was calculated only when a FISH signal for both probe sets (based on Tm and $\Delta G_{37^\circ\text{C}}$) was available.

2. Supplementary Protocol: mRNA detection with smiFISH

Primary probe-set preparation

Primary probes are produced in 96-well plates. For convenience, the oligonucleotides are delivered wet and frozen in Tris-EDTA pH 8.0 (TE) buffer, at final concentration of 100 μ M. Prepare an equimolar mixture of 24 primary probes, and dilute the mixture 5 times in TE buffer (final concentration of individual probes is 0.833 μ M).

FLAP preparation

The fluorescent FLAP is delivered lyophilized. Resuspend the FLAP in TE buffer at final concentration of 100 μ M. For long-term storage, make aliquots and store at -20°C in the dark.

Flap hybridization reaction

The hybridization of the probe-set with the FLAP can be performed *i*) in a PCR machine (cycler), or *ii*) on a heating block.

Cycler:

- Prepare the reaction mix according to **Table P1** below.
- Incubate reaction mix in a cycler according to **Table P2**.
- Put sample tubes on ice. For long-term storage, keep hybridized duplexes at -20°C.

Heating block:

- Prepare the reaction mix as in **Table P1** by scaling up the reaction volume to 20 μ L.
- Incubate reaction mix in a heating block 3min at 85°C.
- Turn heater off and incubate sample tubes until temperature drops to \approx 35-40°C.
- Put sample tubes on ice. For long-term storage, keep hybridized duplexes at -20°C.

N.B. While in the heating block, protect samples from light.

The hybridized flap-structured duplexes can go through multiple freeze-thaw cycles (2-5), without decrease of signal.

<u>Component</u>	<u>Volume per reaction</u>	<u>Amount</u>
Probe-set* ¹	2 μ L	40 pmol (total amount of DNA)
100 μ M FLAP	0.5 μ L	50 pmol
10X NEB 3* ²	1 μ L	
H ₂ O	6.5 μ L	

Table P1: FLAP hybridization reaction mix (for cycler)

*¹ Probe-set: equimolar mixture of 24 probes (see step *Probe-set preparation*)

*² NEB 3: New England Biolabs Buffer 3 (1X composition: 100mM NaCl, 50mM Tris-HCl, 10mM MgCl₂, pH 7.9)

<u>1 cycle:</u>	85°C	3min
<u>1 cycle:</u>	65°C	3min
<u>1 cycle:</u>	25°C	5min
Lid :	99°C	

Table P2: Incubation of *FLAP hybridization* reaction mix in a cycler

Plating cells and fixation

Day 1:

1. Plate cells on coverslips in 6-well plates to be 60-70 % confluent the next day.

Day 2:

2. Remove medium and rinse cells once with PBS
3. Fix with 4% paraformaldehyde (freshly prepared in PBS) for 20 min at RT
4. Rinse twice in PBS
5. Permeabilize in 70% ethanol overnight at 4°C, with a Parafilm sheet wrapped around the 6-well plate. At this step, cells can be stored at 4°C for several weeks provided coverslips do not dry.

In situ hybridization (Day 3):

6. Rinse cells once with PBS
7. Incubate in 15% formamide freshly prepared in 1X SSC buffer for 15 min at RT
8. During incubation time, prepare *Mix 1* and *Mix 2* on ice according to **Table P3**. A volume of 100µL (*Mix 1* + *Mix 2*) is sufficient for two coverslips (22 x 22 mm).
9. Vortex thoroughly *Mix 2*. Then add *Mix 1* to *Mix 2* and vortex again.
10. Drop 50µL of the hybridization mix on a 10cm Petri dish and lay the coverslip on the drop (cells facing down). Be careful to avoid air bubbles.
11. Put a 3.5cm Petri dish containing 1mL of 15% formamide/1X SSC solution inside the 10cm Petri dish, wrap a Parafilm sheet around the Petri dish, and incubate at 37°C overnight.

<u>Component</u>	<u>Volume per 100µL (<i>Mix 1</i> + <i>Mix 2</i>)</u>
<i>Mix 1</i>	
20X SSC	5µL
20µg/µL <i>E. coli</i> tRNA	1.7µL
100% formamide	15µL
Flap-structured duplexes* ¹	2µL
H ₂ O	26.3µL
<i>Mix 2</i>	
20mg/mL RNase-free BSA	1µL
200mM VRC* ²	1µL
40% dextran sulphate	26.5µL
H ₂ O	21.5µL

Table P3: *In situ* hybridization reaction *Mix 1* and *Mix 2* (for two coverslips 22 x 22 mm)

*¹ For preparation of Flap-structured duplexes see step *FLAP hybridization*.

*² VRC: vanadylribonucleoside complex

Washing and mounting (Day 4):

12. Place the coverslips inside a 6-well plate and wash the cells twice for 30min in freshly prepared 15% formamide/1X SSC at 37°C.
13. Rinse twice in PBS before mounting.
14. Drop 10µL of Vectashield mounting medium containing DAPI on the slide and lay down the coverslip on the drop (the surface of the coverslip containing the cells should face the drop), and remove excess medium with Kimwipes.
15. For long-term storage, keep slides at -20°C.

Note: we obtained also good results with an alternative hybridization buffer (100 mg/mL dextran sulfate and 10% formamide in 2X SSC). Also, smiFISH is compatible with the new smFISH buffers offered by Stellaris (Biosearch).

Detection of mRNA by dual-colour smiFISH

Two kinds of Flap secondary probes are used, conjugated to either Cy3, Cy5, or digoxigenin, allowing immunofluorescence detection with anti-digoxigenin-fluorescein Fab fragments.

Flap hybridization reaction and in situ hybridization

Proceed as above, with both types of Flap structured duplexes added to *Mix 1* in equal amounts.

Immunofluorescence

- Permeabilize the cells with 0.1% Triton-X100/PBS for 10 minutes at RT.
- Wash with PBS.
- Incubate with anti-digoxigenin-fluorescein Fab fragments diluted to 0.25 µg/ml in PBS for 2 hours at RT.
- Wash with PBS and mount samples as previously described.

List of reagents

- 10X NEB 3 (New England Biolabs)
- 1X PBS (Lonza)
- PFA (paraformaldehyde, Electron Microscopy Sciences)
- 20X SSC buffer (3M NaCl, 0.3 M sodium citrate, pH 7)
- *E. coli* tRNA (Sigma)
- 100% formamide (Sigma)
- 20mg/mL RNase-free BSA (Roche Diagnostics)
- 200mM Vanadylribonucleoside complex (Sigma)
- 40% dextran sulphate (Dextran Sulfate Sodium Salt, MP Biomedicals, LLC)
- Vectashield antifade mounting medium with DAPI (Vector Laboratories)
- Anti-digoxigenin-fluorescein, Fab fragments (Roche)

3. Note 1: sequences of FLAP probes

FLAP X-Cy3	/5Cy3/C ACT GAG TCC AGC TCG AAA CTT AGG AGG/3Cy3Sp/	28 nt
FLAP Y-Cy3	/5Cy3/AA TGC ATG TCG ACG AGG TCC GAG TGT AA/3Cy3Sp/	28 nt
FLAP Y-Cy5	/5Cy5/AA TGC ATG TCG ACG AGG TCC GAG TGT AA/3Cy5Sp/	28 nt
FLAP Z-Cy3	/5Cy3/CTT ATA GGG CAT GGA TGC TAG AAG CTG G/3Cy3Sp/	28 nt

Sequences of the fluorescent FLAPs (secondary probes) used in the study. The probes are conjugated to two Cy3 or Cy5 moieties at the 5' and 3' termini. The symbols used by IDT corresponding to each modification are shown. The length of the probes is indicated. nt: nucleotides.

4. Note 2: Oligostan – R script for probe design

We have developed a script with R (5) to extract specific smiFISH probe sequences for sequences of interest. The script uses the R packages “seqinr” and “zoo”.

Oligostan runs on all major operating systems (Window, Macintosh, Linux). However, the option to mask repeated sequences with RepeatMasker (6) is only available for Macintosh and Linux. On Windows systems, repeated sequences can be masked before using Oligostan, for instance on the following website <http://www.repeatmasker.org/cgi-bin/WEBRepeatMasker>.

Oligostan is available with a detailed helpfile and tutorial at https://bitbucket.org/muellerflorian/fish_quant.

5. Note 3: fully automated analysis workflow for smFISH images in

Overview

We recently developed the software package FISH-quant dedicated to the automated analysis of single-molecule Fluorescence in situ Hybridization (smFISH) images (1). In brief, this software allows detecting spots from 3D microscopy images with high precision and exports the location of these spots. However, a recurrent bottleneck in the analysis was the manual definition of cellular outlines, which limited the use of FISH-quant to low-throughput studies. Here, we present a new projection method to generate 2D images based on global and local focus measurements from 3D microscopy data. This method yields crisp images with sharp cell boundaries, which yield better segmentation results with standard tools than traditional projections, such as average or maximum projections. An equally important step in the analysis of smFISH images is the mRNA detection. A number of methods have been proposed in the literature, but they have not been carefully compared yet and consequently, the choice of which method to use is not obvious. We therefore implemented these methods and compared their performance on realistic, simulated images with known ground truth. We further provide explanations and guidelines for how to use the best method.

In summary, we now provide a complete analysis framework for smFISH images from automated cell segmentation to mRNA detection as detailed below. We implemented these tools in MATLAB and provide Graphic User Interfaces to easily go through all the steps of the complex analysis workflow.

Improved cell segmentation by focus based projection

Automatic cell segmentation is essential to efficiently treat large volumes of data, especially in the context of High Content Screening (HCS). Even if images are acquired in 3D, segmentation is routinely performed on 2D projections, in particular in the absence of a cell membrane marker. A number of efficient and well established 2D segmentation algorithms have been developed (7–9) and are distributed to the scientific community through open-source software platforms (3, 8) and we therefore based our analysis pipeline on these existing tools. However, we found that one aspect of the typical workflow – the projection method transforming a 3D image stack into a 2D stack – can have a profound impact on the downstream quality of the segmentation and can be further improved. Indeed, voxels in a 3D stack typically receive large contributions of out-of-focus signal (Fig 1). The rather homogenous non-specific cellular staining is due to non-specific binding of the smFISH probes.

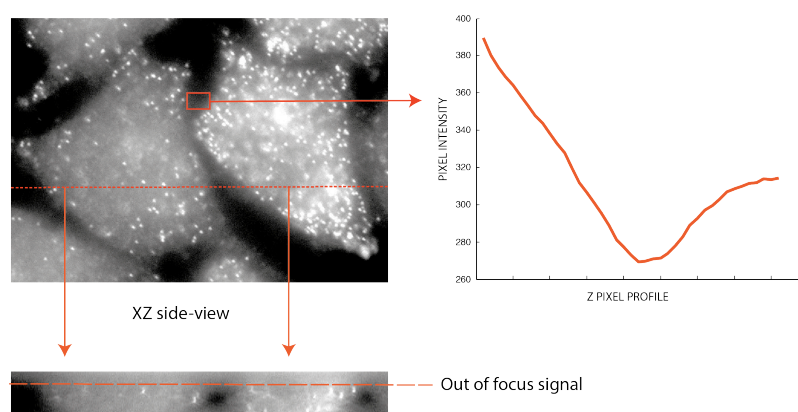


Figure 1 | Presence of out-of-focus slices and impact on the background signal. Images on the left show smFISH against KIF5B in HeLa cells. Image on the top is a maximum intensity projection along Z, image on the bottom is the view of the image along the XZ plan. Plot on the right shows averaged pixel intensity in the red rectangle as a function of the z-position. This region does not contain any cells but shows intensity variations. Intensities increase towards the extremities of the z-stack. This increase is due to out-of-focus signal – as can be seen on the side-view.

Performing a standard maximum intensity projection along z on this image, will result in a 2D image,

where each pixel will be assigned with the maximum value of all pixels of sharing the same XY position. While this process will yield a good signal for bright cellular structures, it will result in blurred cellular boundaries due to contributions of out-of-focus light, as XY positions outside the cellular region will receive out-of-focus signal from other slices even though no fluorophore is situated at this position. This will result in less reliable detection of the cellular boundary by the downstream segmentation method. Here, we present a new projection method that uses global and local focus measurements to circumvent this problem, and obtained projected images with high contrast allowing an accurate segmentation. In short, we first use a global focus measurement to automatically remove out-of-focus slices. Second, we use a local focus measurement to determine for each pixel from which z-slices the intensities values should be considered in an averaging operation.

Global focus measurement to remove out-of-focus slices

The focus of an image or a region of an image can be quantitatively assessed by determining contrast or sharpness features of the acquired images. If such measurements are taken for a series of images at different z-positions, the focus measurement should take its maximal value when the corresponding image is in focus. Many different operators for focus measurement have been proposed, e.g. using gray level variability, local contrast, or more recently, wavelet decomposition (10). It has been shown (11) that these operators provide very different results depending on the type of images (nuclei or cells) and other parameters such as cell density, signal intensity, etc.

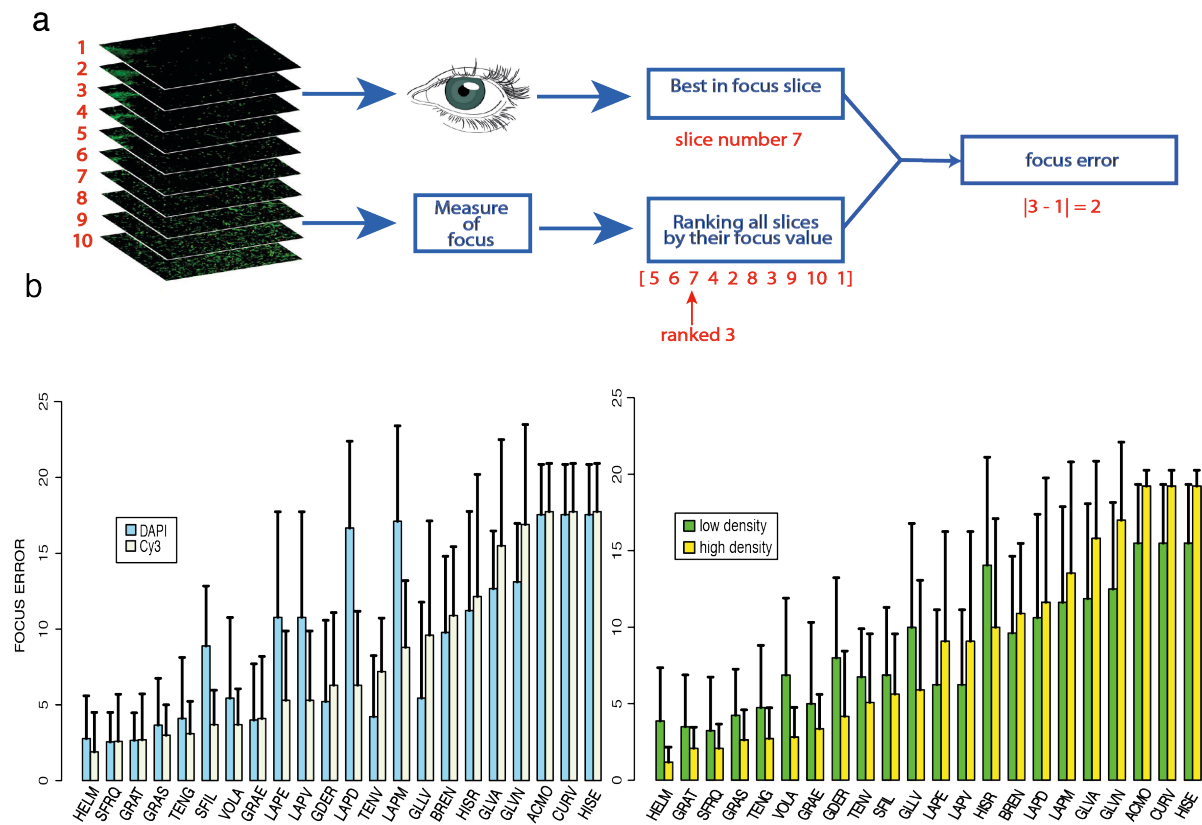


Figure 2 | Measurement error for different focus operators. (a) The results of the focus operators are compared to a manually obtained ground truth. Slices are ranked by their measured focus value and the focus error is defined as the rank of the visually determined best slice minus 1 (example in red text). (b) Bar plot of mean and standard deviation of focus error for Cy3 and DAPI images (left) and different cell densities (right; Cy3 and DAPI were grouped). 5 operators gave satisfying results with a mean ranking error lower than 5 for both Cy3 and DAPI. The focus error is higher in images with low cell density.

We therefore first compared the performance of a collection of focus measurement operators (11) on images representative for our assay. We assembled a diverse test data set with smFISH and DAPI

images with large variations in terms of cell density, cell types, and signal intensities. We used smFISH images since these can serve for cellular segmentation due to the signal stemming from the non-specific staining of the FISH probes as seen in Fig 1. We manually determined the best in-focus slide for each of these 3D images. We then applied to each image each of the focus measurements to automatically rank the 3D slices based on their focus. To determine the quality of this automated measurement, we calculated the ranking error for each method. This error is simply determined as the rank of the best in-focus slide minus 1 (Fig 2a). For example, if the manually best slide were ranked by a method as the 5th best slide, the ranking error would be 4. As previously reported (11), we also observed considerable variability between the different operators, but we also observe that some focus measurements seem to recapitulate our visual inspection in different scenarios. We therefore conclude that they can be used efficiently to distinguish between in-focus slices and out-of-focus slices for our images.

We used these operators in a first processing step to **automatically remove out-of-focus slices**, resulting in a 3D stack with a reduced number of slices. The number of slices that are kept is adjusted to approximately correspond to the thickness of a typical cell. While this could be done manually for a few images, such a manual inspection would be extremely time-consuming for large data sets.

Local focus measurements for improved 2D projection

We then measured focus locally by assigning to each voxel $v=(x,y,z)$ the focus measurement calculated on the z-slice in a small neighborhood centered in (x,y) . This measurement is obtained by moving a small window with a user-defined size over each XY slice (Fig 3a). The focus within this region is calculated and assigned to each voxel. We used the Matlab function *focusmeasure* provided in Pertuz et al. The result is a 3D matrix with the same size as the original image. Each element corresponds to the local focus measurement of a pixel in the corresponding z-slice. To perform a 2D projection, voxel-values in the original 3D stack can be chosen based on these local focus measurements. In a qualitative inspection of the data, we observed that the local projection yields sharper cell boundaries (Fig 3b-c), providing potentially better input images for cell segmentation algorithm.

Segmentation of smFISH images

We next wanted to test the impact of these different projection strategies on real smFISH images. As ground truth, we used the data set (around 100 cells) from above and manually drawn outlines from 3 experienced microscopists.

We implemented two different local projections by assigning to each XY position (a) the value of the z-slices with the maximum focus value; (b) the median value of the 5 z-slices with the highest focus measurement. We combined this with the out-focus slice removal from above, to define 5 different projections strategies:

- (S1) Entire stack: maximum intensity projection;
- (S2) 30% best in-focus slices; median projection
- (S3) 75% best in-focus slices; local focus (7x7 window); maximum focus value
- (S4) 75% best in-focus slices; local focus (15x15 window); maximum focus value
- (S5) 75% best in-focus slices; local focus (7x7 window); median projection of the 5 highest focus values.

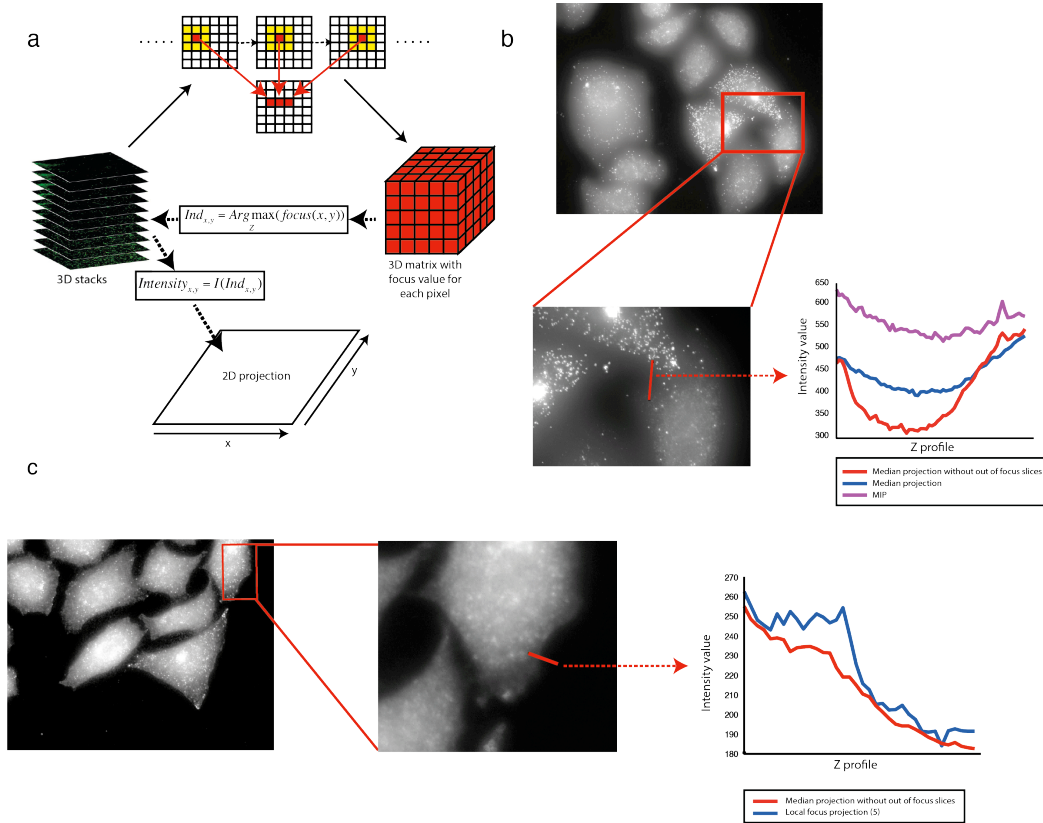


Figure 3 | 2D projection based on single pixel focus measurement. (a) Single pixel focus measurements are calculated by moving a window over each XY slice of the 3D stacks. The 2D projection is then established based on the single-pixel focus measurement. In the example the pixel-values for each XY position with the highest focus value along Z are chosen. (b) Z axis profile shows the benefits of out of focus slices removing step to get sharper cell boundaries. (c) Z axis profile shows that the cell boundaries are even sharper when combining the out of focus slices removing step with the single pixel focus measurement.

These 2D projections were then processed with *CellCognition* (3) using two different segmentation algorithms:

- (1) Propagation from the nucleus combined with local Otsu image thresholding;
- (2) Watershed segmentation combined with global image thresholding.

To quantitatively compare the segmentation results, we implemented different metrics to judge the accuracy of the segmentation for the cell area and the cell boundary. For the cell area, we calculated:

$$(1) \quad \text{DICE coefficient} = 2 \frac{\#(A \cap M)}{\#A + \#M}$$

A and M are the automatically (A) and manually segmented (M) regions that are compared, # denotes the number of pixels inside the region. Hence, the DICE coefficient is a measure of similarity between these two regions. It goes to zero if the regions do not overlap at all, and to one if they are identical.

Furthermore, let TP be the number of true positives (pixels detected both manually and automatically), FP the number of false positives (pixels detected automatically but not manually) and FN the number of false negatives (pixels detected manually but not automatically). We can then define **precision** as the probability that an automatically selected pixel is also manually selected:

$$(2) \quad \text{Precision} = \frac{TP}{TP+FP}$$

Furthermore, we can define **sensitivity** (also known as recall) as the probability to automatically detect a manually selected pixel:

$$(3) \quad \text{Sensitivity} = \frac{TP}{TP + FN}$$

The metrics were applied to the surface of a segmented cell. However, cells can have thin protrusions with a small surface compared to the entire cell. Metrics based on area comparison will not be very sensitive with respect to the detection of these protrusions. We therefore implemented similar metrics for the **cell boundary**. Based on the segmented outline, we consider a tube (with a radius of 18 pixels; as a comparison the typical diameter of a cell is between 200 and 300 pixels) representing a confidence interval of detection (Fig 4a). When doing this for the manually segmented cell membrane, we can determine how many pixels of the automatically segmented membrane are located within this region. This allows measuring FP (pixels belonging to the automated cell membrane outside the tube), TP (pixels belonging to the automated cell membrane inside the tube) and FN (pixels belonging to the manual cell membrane outside the tube) and consequently the calculation of precision and sensitivity as defined above.

Lastly, we compared the quality of manual segmentation provided by different human graders by applying these measurements to pairs of cells segmented by the different biologists.

We then compared the quality of the different projection strategies and segmentation algorithms (Fig 4c-g). This allowed several observations: first, the watershed methods worked in general better than the propagation method (Fig 4c). Further, the local focus projection yielded a significant improvement of the quality of the segmentation for both the area and border (Fig 4d-g). The overall best results were obtained with projection strategy 5, i.e. with a local focus that considers the median value of the 5 best in-focus slices in z for each xy position. This improvement can be appreciated in Figure 5 where protrusions (Fig 5a) were successfully detected in the local focus projection (Fig 5c) but not in a standard maximum intensity projection (Fig 5b).

In summary, the local focus projection provides a simple method to increase the quality of projection of 3D images used in nuclear and cellular segmentation. This increased quality improves the segmentation results, approaching the results obtained by a manual segmentation.

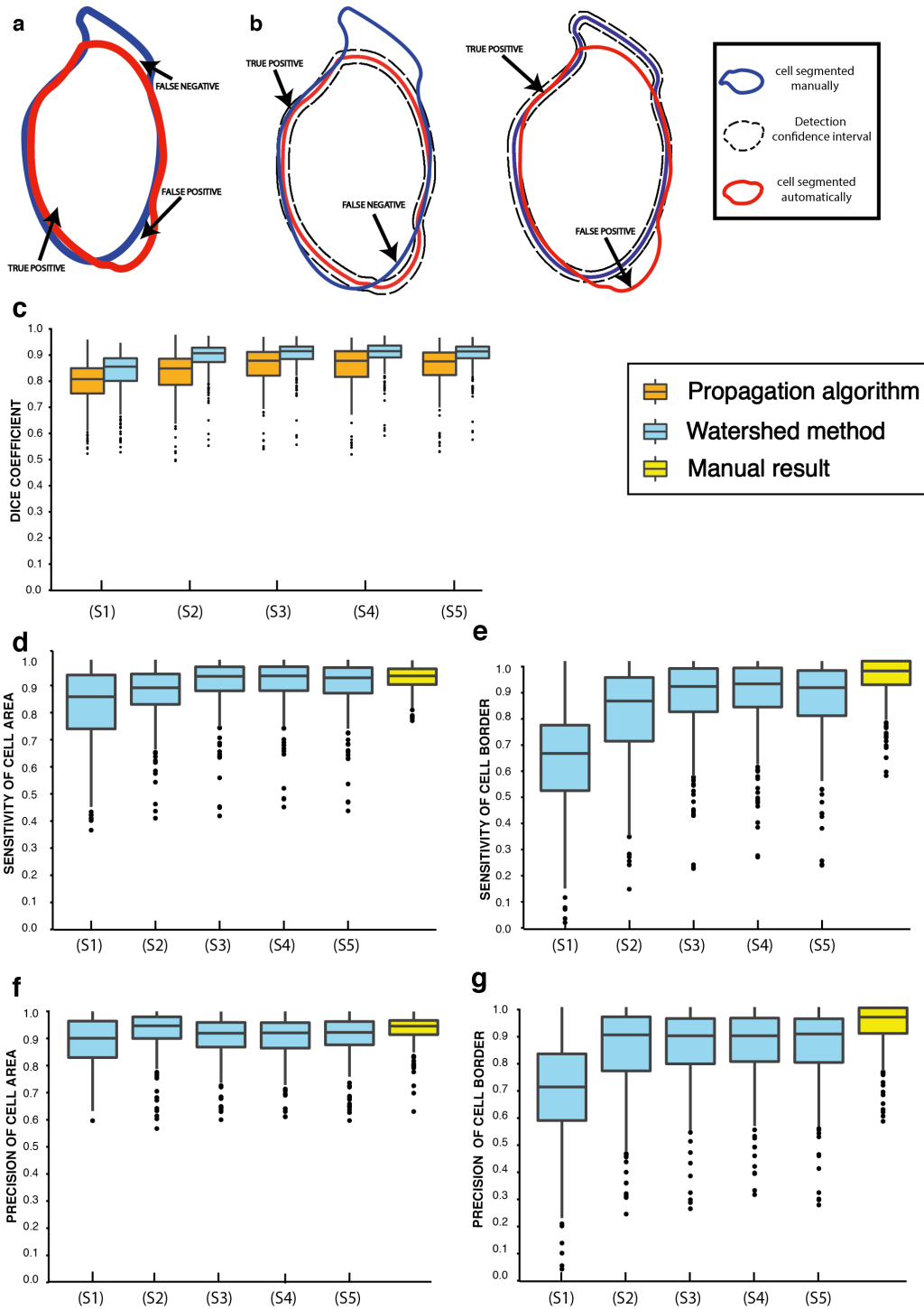


Figure 4 / Comparison of segmentation results for different projection methods. (a-b) True positive, false positive and false negative for cell area and cell boundary are defined to calculate sensibility and precision of the segmentation. For cell border measurement detection confidence intervals are defined around the border of automatically and manually segmented cells. (c-g) The (1),(2),(3),(4),(5) in the plots correspond to the projection strategies describe above. The boxplots show the median inside the box defined by the 25th and the 75th quantiles, and whiskers defined by a difference of more than 1.5 times the IQR (Interquartile range, equivalent to the box length) (c) Comparison of the results of DICE coefficient for the 5 projections methods and for two different segmentation algorithms. The watershed algorithm gives better results applied on any projection. We see a global improvement of the segmentation results by using focus measurement instead of MIP. Using focus measurement slightly increases the median of DICE and reduces the variability. (d) The strategies using local focus measurement (3,4,5) give the best results, with a slight improvement of the median and a reduction of variability. (e) Focus strategies present a significant improvement of cell border sensitivity compared to the MIP. Local focus strategies reduce the variability. (f) Overall good results for the cell area precision. (g) Focus measurement strategies show an improvement of the cell border precision.

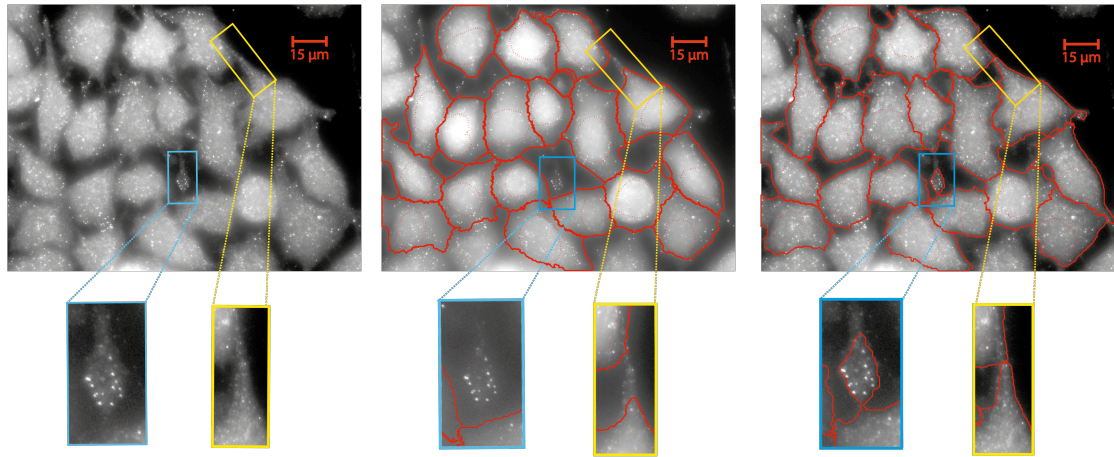


Figure 5 | Segmentation results for different projection. (Left) smFISH image with protrusion visible due to mRNA localization as shown in the two zoom-ins. (Middle) Segmentation result based on maximum intensity projection. (Right) Segmentation result with focus projection strategy 5.

General applicability

We tested our approach on different images and model systems to demonstrate its general applicability. First, we successfully segmented smFISH images from yeast and DAPI images from embryonic stem cells. (Fig 6a-b). Second, we applied our approach to images obtained with a non-specific cell marker (*CellMask*), which is widely used for high-content screens. While cells are nicely stained with this marker, we found that the cellular boundaries are shaper after application of the local focus projection (Fig 6c).

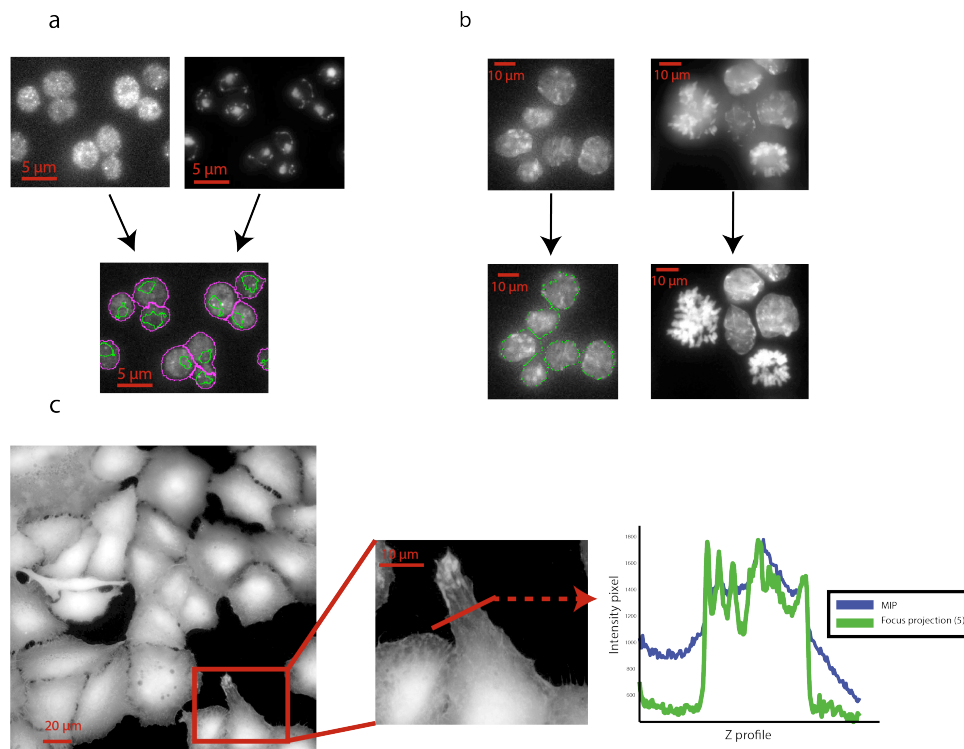


Figure 6 | Segmentation of different types of images. (a) Stellaris FISH RNA probes (Quasar570-labelled) directed against the GFP sequence of a synthetic reporter (left) DAPI (right). Lower image shows segmentation with CellProfiler (cells in pink, nuclei in green). Images by Estelle Dacheux (University of Warwick) (b) Nuclei in ES cells stained with DAPI. Maximum Intensity projection (upper images) and focused projection (lower images). Green outlines show segmented cells. Images by Philippe Clerc (Pasteur Institute) (c) A549 cells stained by HCS CellMask™ Green stain (H32714) displayed with logarithmic contrast. Zoom-in shows magnification of a cell. Plots show intensity profile along the red line. Green after focus projection, blue after a maximum intensity projection. Image by Benjamin King (University of Vermont).

Implementation in FISH-quant

We now provide a dedicated graphical user-interface that allows creating these projections. They can then be analysed either in *CellCognition* or *CellProfiler*. These programs create segmentation masks that can then be converted in FISH-quant outline files. For more details please refer to the separate documentation in FISH-quant.

Comparison of spot detection methods

Overview

The central part in the analysis of smFISH images is the detection and localization of individual mRNA molecules. A number of different methods have been proposed, which commonly share two important processing steps (i) filtering of the image to remove background and increase the signal of individual spots (ii) detection of spots.

Two commonly used filters are

1. **Laplacian of Gaussian filter (LoG)** (2). This filter works by first smoothing the image with a Gaussian kernel and calculating the Laplacian (based on the second derivative of the image) of the smoothed image (Fig 7a).
2. **Dual Gaussian filter** (1). This filter performs a two-step convolution using Gaussian kernels (Figure 7b). First, the background is estimated using a large Gaussian kernel (usually five times larger than the PSF) and subtracted from the image. Then, this background-subtracted image is convolved with a small Gaussian kernel to increase the signal-to-noise ratio of the mRNA spots.

Usually, the signal of individual mRNA molecules is very bright, so rather simple detection methods routinely work well. Specifically, two approaches have been widely used.

1. **Connected components** (2, 12) (**Fig 7c**). The image is first binarized based on a user-defined threshold. Then connected pixels are defined as regions and each of these regions is considered to be a mRNA molecule. This method suffers from detecting several spots as one object, when the mRNA density is high. Recently, a further modification of this approach has been proposed allowing the separation of closely located spots that are detected as one larger region (12). This “deblending algorithm” can be applied on detected regions to split them into individual spots. For every region, the algorithm applies multiple thresholds starting from the initial detection threshold to the maximum value of the image, and decides each time the threshold separates a region if the separation is relevant and if the parts should be considered as independent spots.
2. **Local maximum** (1) (**Fig 7d**). This method relies on the detection of local maxima, which are defined by two criteria. First, they are brighter than a user defined threshold. Second, they are brighter than all other voxels in a user-defined window surrounding them. This window size can play a critical role when working with dense images. For instance, a bright spot might not be detected because another bright spot is found in close proximity.

One important aspect for both methods is determining the **optimal intensity threshold**. For smFISH image analysis, no fully automated method to determine this threshold has been proposed so far in the field of smFISH image analysis, but a simple sequential test of different thresholds provides a good guideline. The analysis software tests a number of intensity thresholds and records the number of detected spots. The curve displaying number of detected spots as a function of the intensity threshold, has very low values for high thresholds (under-detection), and very high values for low thresholds (over-detection). Depending on the detection method, this curve is not necessarily monotonic and in particular, the number of detected objects might decrease again for extremely low thresholds, as different spots connect to each other. For the intensity values corresponding to real mRNA molecules,

usually a characteristic plateau can be seen (1, 2). This intensity value is usually constant for a given experiment, but may change from experiment to experiment even for the same target gene due to variability in the smFISH experiments.

Further, detection methods can be applied directly on the **3D** stacks (1) or on a **2D maximum intensity projection** (2, 12). The advantage of 2D images is the reduced data volume and increase in processing speed. The downside is that spots overlapping in 3D might not be distinguished anymore.

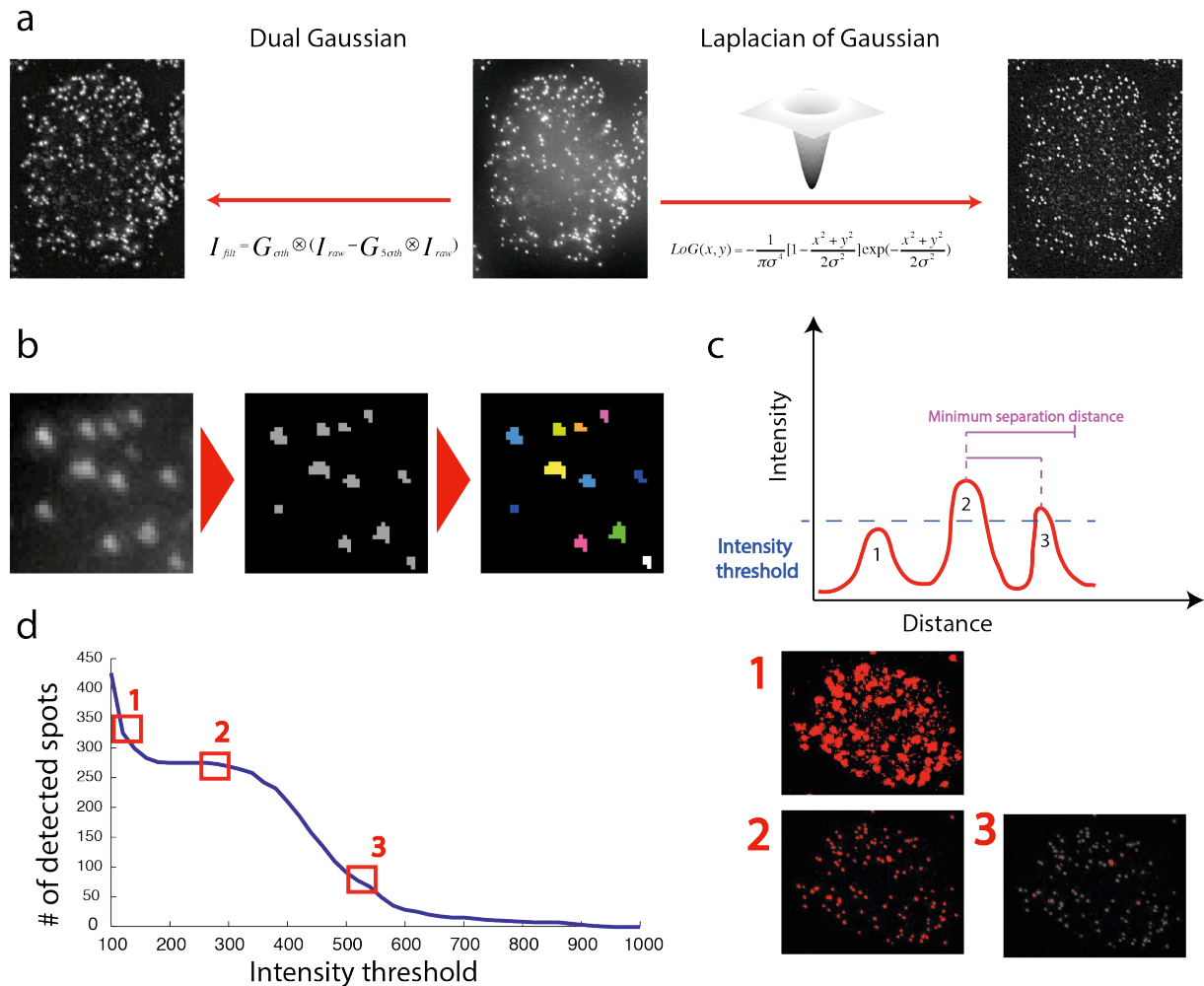


Figure 7 | Overview of important steps during mRNA detection. (a) Laplacian of Gaussian filtering (right), Dual Gaussian filter (left), Raw smFISH image (middle) (b) Connected component (right) are detected on a thresholded image (middle). Each detected region is colour-coded. Image is shown in 2D but analysis can be performed in 3D. (c) Local maximum detection. A maximum is only considered if it is brighter than the threshold (1 is too dim) and no other brighter maximum is within a user defined distance (maximum 3 is not considered because the brighter maximum 2 is closer than the user defined distance). Illustration is in 1D but analysis is performed in 3D. (d) Dependency of number of detected spots on the detection threshold. Figures on the right show examples for different thresholds as indicated by the numbers. Results of connected components in red and the smFISH image in gray. 1-over-detection; 2-good detection; 3-under-detection.

Performance comparison of detection methods with simulated smFISH images

Different combinations of these filtering and detection approaches have been successfully used in the past. However, to our best knowledge, neither a careful comparison of their performance for smFISH images nor guidelines for the use of these methods have been published so far. In order to have a well-defined ground-truth, we simulated realistic smFISH images with precise control about how many mRNA molecules are present.

In short, we start from an empty background image where we add a known number of mRNA molecules at random localization in 3D. We then analyse these images with the different detection methods and can compare not only if the method correctly estimated the number of molecules but also if they retrieve the correct positions. To obtain realistic images, we considered 4 important points.

First, individual mRNA molecules are usually diffraction-limited in **size** (1) and can therefore be described by the point-spread function (PSF). To simulate a realistic PSF, we used the ImageJ plugin *PSFgenerator* (13). However, it has been reported that these theoretical PSF models yield PSFs that are smaller than the actual PSF as measured on an optical setup (14). We therefore first investigated if this applies to our experimental setup. We detected several hundred individual mRNA molecules in a typical smFISH image and calculated an averaged image using FISH-quant(1). We fit this image with a 3D Gaussian function and estimated its variance σ_{xy} in XY and σ_z in Z. We then simulated a PSF assuming the parameter of our microscope with the ImageJ plugin *PSFgenerator* (13) and also estimated the variance of a 3D Gaussian fit. When comparing these estimates, we noticed a size difference between the simulated and the observed PSF, which was in agreement with the values reported previously(14):

$$F_{xy} = \frac{\sigma_{xy, simulated}}{\sigma_{xy, real}} = 1.3 \quad \text{and} \quad F_z = \frac{\sigma_{z, simulated}}{\sigma_{z, real}} = 1.6.$$

We considered this size difference in our simulation, by generating the PSF with corrected pixel size. We want to simulate a PSF of a microscope setup with 63X objective and pixel size of 102nm in xy and z-step size of 300nm. In order to correct the difference of size between simulated and observed, we therefore simulated on a smaller pixel grid with 63.75 nm in xy and 187.5 nm in z.

Second, in real images molecules have different **sub-pixel locations** yielding different diffraction limited images even if the underlying PSF is the same. To consider this effect we generated the PSF on a finer pixel grid than the grid of the final image. The simulated smFISH image has therefore also a smaller pixel grid. In a final step, this image will be binned, e.g. groups of pixels are replaced by a larger pixel with the mean value of the underlying smaller pixels (Fig 7a). The individually placed PSF will then have slightly different underlying center coordinates mimicking different sub-pixel (Fig 7a).

Third, individual mRNA molecules show a distribution of **intensity values**. This distribution stems from many factors including labelling and hybridization efficiency (1). To mimic realistic mRNA molecules, we extracted the distribution of the intensity of single mRNA and fitted it with a skewed normal distribution (Fig 7b) as reported previously (1). When simulating individual mRNA molecules, we assigned an intensity value drawn from this empirical distribution.

Forth, in smFISH images usually a pronounced background can be observed due to non- or semi-specific binding of individual probes. To consider this in our simulations, we used the image of a cell not expressing any mRNA as background for our simulation (Fig 7c). Addition of individual mRNA molecules was restricted to the region corresponding to this cell.

Comparison of different detection strategies

We simulated smFISH images with increasing number of mRNA molecules and quantified these images with different analysis workflows. We first compared the detection efficiency of analysing 3D images vs. 2D maximum intensity projections on Dual Gaussian filtered images (Fig 8d). For simulations with a low mRNA count, the correct number was inferred. However, at higher mRNA levels only around 40% of all spots were detected when using 2D projections. Surprisingly, the deblending algorithm did not increase the efficiency substantially (blue curve in Fig 8d). On the other hand, the local maxima approach detected a substantially higher fraction of spots (70%, see Fig 8d), when applied on the 3D stacks indicating that using 3D stacks probably results in more accurate results.

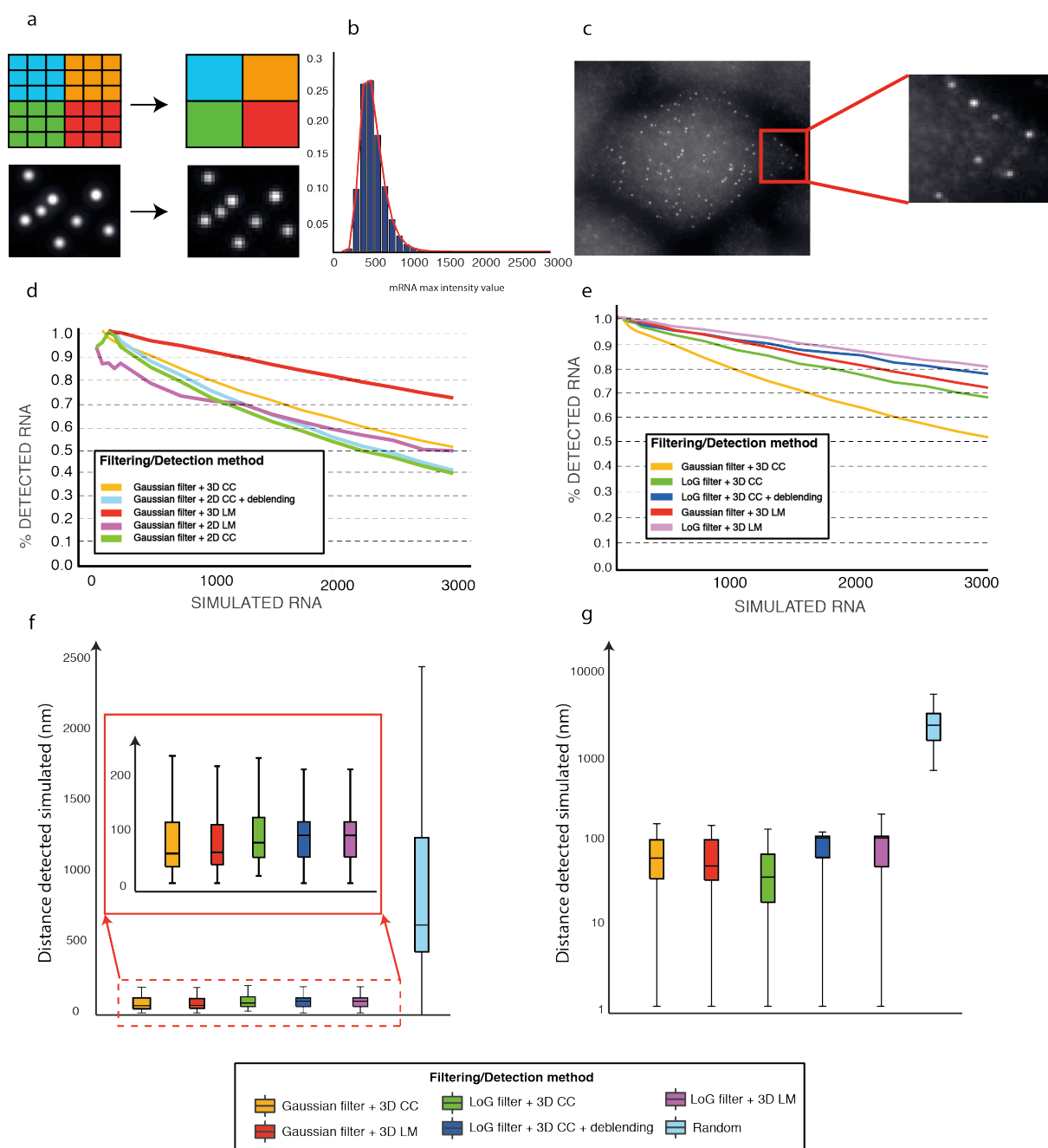


Figure 8 | Comparison of single RNA detection method on simulated images. (a) Single molecules are simulated on a finer pixel grid which is then binned to obtain the final image. This yields different signals for individual molecules due to their different sub-pixel center position. (b) Distribution of smFISH spot intensity is extracted from real images with FISH-quant and fit with a skewed normal distribution. Intensity of a spot is defined as the maximum pixel value of the spot above background. The density curve is generated with the Matlab function *pearsrnd*. (c) Example of simulated image. Each spot has a random intensity following the distribution in (b) and are added at a random location to the image of cell with no target mRNA expressed. (d) Comparison of 2D and 3D detection after difference of Gaussian filtering. Shown is the percentage of detected spots as a function of the known number of detected spots. (e) Comparison of different detection strategy combining in 3D for LoG and Gaussian filter. (f-g) Distance between each detected mRNA and the closest simulated mRNA molecule for different mRNA levels (50 (f) and 3000 (g) mRNA per cell). Random control was obtained by choosing randomly 50 (f) or 3000 (g) pixels in the image and treat them as detected spots.

We therefore focused on methods applied to the 3D stacks. We found that the LoG filter can yield higher detection efficiencies compared to the Dual Gaussian filter (Fig 8e). Further, local maximum strategy outperforms the basic connected component strategy (violet vs. green and red vs. yellow in

Fig. 8e). It is important to note that for the LM detection we set the detection window to the smallest possible size, i.e. ± 1 voxel in all directions. The overall best detection was therefore performed by the LM method applied on a LoG filtered image. We note however, that the deblending substantially improves the results of the connected component strategy such that it can be seen as a competitive alternative to the LM method (blue curve in Fig. 8e).

We finally wanted to verify that the detected mRNAs indeed correspond to the simulated mRNAs and not false-positives. To this end, we determined the colocalization between detected and simulated spots detected (See Figure 8f-g). For each detected spot, we calculated the distance to the closest simulated spot. False detection will have larger values, as shown by random controls. Our results indicate, that the mean accuracy is less than a pixel for the different tested methods and substantially smaller than the random control. This shows that most of the detected spots are not false detections and the position of the real spots is accurately estimated.

In summary, we conclude that the local maximum detection combined with the Laplacian of Gaussian strategy provides the best method among the tested approaches to reliably and accurately count and localize individual mRNA molecules in smFISH images. The connected component approach is an acceptable alternative when combined with a deblending strategy.

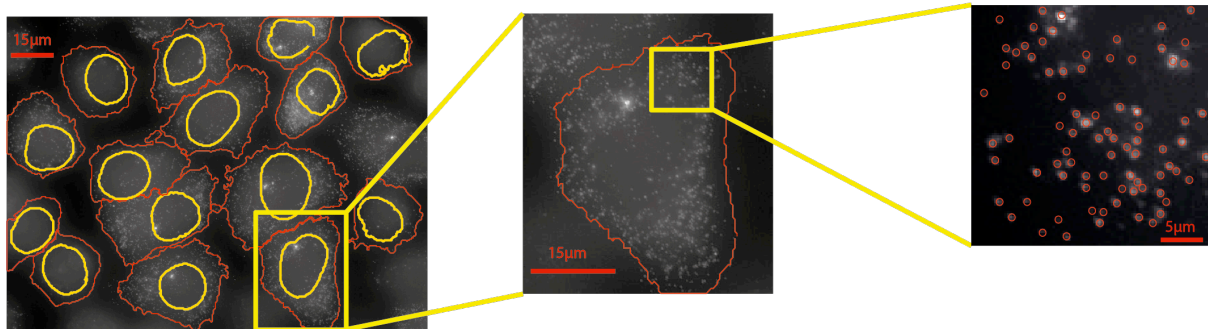


Figure 9 | Result of segmentation and spot detection. Segmentation is performed with watershed algorithm applied on a local focus projection (Cells are red, nuclei are blue). Spot detection is performed with local maximum detection method applied on Laplacian of Gaussian filtered image (each detected mRNA is shown as a circle).

Summary

We have developed a complete analysis pipeline for smFISH images allowing to automatically performing single molecule detection in single cells (Fig 9). Here, we present a 2D projection method based on focus operators that significantly increased the segmentation accuracy. By realistic simulations of smFISH images, we determined the detection method yielding best results. The differences were particularly pronounced for regions with high mRNA density. We implemented these tools in an updated version of *FISH-quant*, which is accessible via the dedicated website https://bitbucket.org/muellerflorian/fish_quant. The segmentation plugins are available in CellCognition.

6. References

1. Mueller,F., Senecal,A., Tantale,K., Marie-Nelly,H., Ly,N., Collin,O., Basyuk,E., Bertrand,E., Darzacq,X. and Zimmer,C. (2013) FISH-quant: automatic counting of transcripts in 3D FISH images. *Nat. Methods*, 10, 277–278.
2. Raj,A., van den Bogaard,P., Rifkin,S.A., van Oudenaarden,A. and Tyagi,S. (2008) Imaging individual mRNA molecules using multiple singly labelled probes. *Nat. Methods*, 5, 877–879.
3. Held,M., Schmitz,M.H.A., Fischer,B., Walter,T., Neumann,B., Olma,M.H., Peter,M., Ellenberg,J. and Gerlich,D.W. (2010) CellCognition: time-resolved phenotype annotation in high-throughput live cell imaging. *Nat. Methods*, 7, 747–754.
4. Hungarian Algorithm for Linear Assignment Problems (V2.3) - File Exchange - MATLAB Central.
5. R Core Team (2015) R: A language and environment for statistical computing. Vienna, Austria; 2014. URL [Httpwww R-Proj. Org](http://www.R-Project.org).
6. Smit,A., Hubley,R. and Green,P. (2013) RepeatMasker Open-4.0.
7. Wählby,C., Sintorn,I.-M., Erlandsson,F., Borgefors,G. and Bengtsson,E. (2004) Combining intensity, edge and shape information for 2D and 3D segmentation of cell nuclei in tissue sections. *J. Microsc.*, 215, 67–76.
8. Kamentsky,L., Jones,T.R., Fraser,A., Bray,M.-A., Logan,D.J., Madden,K.L., Ljosa,V., Rueden,C., Eliceiri,K.W. and Carpenter,A.E. (2011) Improved structure, function and compatibility for CellProfiler: modular high-throughput image analysis software. *Bioinforma. Oxf. Engl.*, 27, 1179–1180.
9. Wang,M., Zhou,X., Li,F., Huckins,J., King,R.W. and Wong,S.T.C. (2008) Novel cell segmentation and online SVM for cell cycle phase identification in automated microscopy. *Bioinforma. Oxf. Engl.*, 24, 94–101.
10. Xie,H., Rong,W. and Sun,L. (2006) Wavelet-Based Focus Measure and 3-D Surface Reconstruction Method for Microscopy Images. In *2006 IEEE/RSJ International Conference on Intelligent Robots and Systems*.pp. 229–234.
11. Pertuz,S., Puig,D. and Garcia,M.A. (2013) Analysis of focus measure operators for shape-from-focus. *Pattern Recognit.*, 46, 1415–1432.
12. Battich,N., Stoeger,T. and Pelkmans,L. (2013) Image-based transcriptomics in thousands of single human cells at single-molecule resolution. *Nat. Methods*, 10, 1127–1133.
13. Kirshner,H., Aguet,F., Sage,D. and Unser,M. (2013) 3-D PSF fitting for fluorescence microscopy: implementation and localization application. *J. Microsc.*, 249, 13–25.
14. de Moraes Marim,M., Bo Zhang, Olivo-Marin,J.-C. and Zimmer,C. (2008) Improving single particle localization with an empirically calibrated Gaussian kernel. In *Biomedical Imaging: From Nano to Macro, 2008. ISBI 2008. 5th IEEE International Symposium on*.pp. 1003–1006.